Conotoxin κM-RIIIJ, a tool targeting asymmetric heteromeric K_v1 channels

Sönke Cordeiro[a,1], Rocio K. Finol-Urdaneta[b,c,1], David Köpfer[d], Anna Markushina[a], Jie Song[a], Robert J. French[c], Wojciech Kopec[d], Bert L. de Groot[d], Mario J. Giacobassi[e], Lee S. Leavitt[e], Shrinivasan Raghuraman[e], Russell W. Teichert[e], Baldomero M. Olivera[e,2], and Heinrich Terlau[a,2]

[a]Institute of Physiology, Christian-Albrechts-University Kiel, 24118 Kiel, Germany; [b]Illawarra Health and Medical Research Institute, University of Wollongong, Wollongong, NSW 2522, Australia; [c]Department of Physiology and Pharmacology, Hotchkiss Brain Institute, University of Calgary, Calgary, AB T2N 4N1, Canada; [d]Max-Planck-Institute for Biophysical Chemistry, Computational Biomolecular Dynamics Group, 37077 Göttingen, Germany; and [e]Department of Biology, University of Utah, Salt Lake City, UT 841120

Contributed by Baldomero M. Olivera, November 16, 2018 (sent for review August 14, 2018; reviewed by Richard W. Aldrich and Michael M. Tamkun)

The vast complexity of native heteromeric K^+ channels is largely unexplored. Defining the composition and subunit arrangement of individual subunits in native heteromeric K^+ channels and establishing their physiological roles is experimentally challenging. Here we systematically explored this "zone of ignorance" in molecular neuroscience. Venom components, such as peptide toxins, appear to have evolved to modulate physiologically relevant targets by discriminating among closely related native ion channel complexes. We provide proof-of-principle for this assertion by demonstrating that κM-conotoxin RIIIJ (κM-RIIIJ) from *Conus radiatus* precisely targets "asymmetric" K_v channels composed of three $K_v1.2$ subunits and one $K_v1.1$ or $K_v1.6$ subunit with 100-fold higher apparent affinity compared with homomeric $K_v1.2$ channels. Our study shows that dorsal root ganglion (DRG) neurons contain at least two major functional $K_v1.2$ channel complexes: a heteromer, for which κM-RIIIJ has high affinity, and a putative $K_v1.2$ homomer, toward which κM-RIIIJ is less potent. This conclusion was reached by (*i*) covalent linkage of members of the mammalian Shaker-related K_v1 family to $K_v1.2$ and systematic assessment of the potency of κM-RIIIJ block of heteromeric K^+ channel-mediated currents in heterologous expression systems; (*ii*) molecular dynamics simulations of asymmetric K_v1 channels providing insights into the molecular basis of κM-RIIIJ selectivity and potency toward its targets; and (*iii*) evaluation of calcium responses of a defined population of DRG neurons to κM-RIIIJ. Our study demonstrates that bioactive molecules present in venoms provide essential pharmacological tools that systematically target specific heteromeric K_v channel complexes that operate in native tissues.

heteromeric Kv-channels | conotoxin kappaM-RIIIJ | Kv1.2

Ion channels open to allow ion flow across an otherwise impermeable membrane. The functional channel protein may consist of a single α-subunit with multiple similarly organized domains (e.g., voltage-gated Na^+ and Ca^{2+} channels) or by the assembly of monomeric α-subunits that associate noncovalently to form the functional pore. Thus, several homologous genes may encode the monomeric α-subunits that comprise a functional ion channel. Examples include TRP (transient receptor potential), K_v (voltage-gated potassium channels), and the ligand-gated channels. In these families, combinations of multiple α-subunit isoforms give rise to a vast array of functional channels.

More than 70 different genes encode mammalian K^+ channel α-subunits constituting the most diverse ion channel family with thousands of potential multimeric arrangements. A central question in integrating the molecular/cellular knowledge into systems neuroscience is which specific complexes of these diverse families are physiologically relevant?

The problem addressing this fundamental question is schematically illustrated in Fig. 1*A*. There, the combination of only two different K_v1 subunits produces six alternative channels with varying levels of functional specialization. Theoretically, the heteromerization of the seven members of the K_v1 family ($K_v1.1$–1.7) investigated here potentially generate hundreds of tetrameric complexes that are virtually indistinguishable in native tissues as the biophysical properties often overlap. The straightforward approach of ablating individual α-subunits (gene knockouts) would result in the functional deletion of all of the different complexes containing that subunit, complicating the interpretation of the resulting phenotypes.

A large body of literature suggests that most neuronal K_v channels are in fact heteromeric combinations of one to four different α-subunits of loosely defined molecular identity. Here, we devised a neuropharmacological strategy to systematically dissect the contribution of single K_v1 α-subunits to heteromeric complexes by exploiting venom peptides that presumably evolved to alter prey behavior and appear "surgically" targeted to specific heteromeric K^+ channel complexes. We have examined the specificity of κM-conotoxin RIIIJ from the venom of piscivorous cone snail *Conus radiatus*, which was initially described as a $K_v1.2$ antagonist (1). The current study provides a thorough assessment of its activity against a variety of $K_v1.2$ containing heteromeric K_v1 channels. The potency and exquisite selectivity of κM-RIIIJ suggests that this peptide evolved to target asymmetrically arranged

Significance

Most ion channels are multimeric (typically comprising 3–5 subunits). The subunits are encoded by homologous members of a gene family, generating an enormous set of possible heteromeric combinations. In this study, we provide evidence that the preferred target of conopeptide κM-RIIIJ is a heteromeric K_v1 channel consisting of three $K_v1.2$ subunits and one $K_v1.1$ or $K_v1.6$ subunit. We define the molecular interaction of κM-RIIIJ with these asymmetric K_v1 channels and show that in dorsal root ganglia (DRG) neurons, different κM-RIIIJ concentrations can distinguish discrete subpopulations of neurons. Our results highlight the potential of natural products and venom components, such as conopeptides, to generally elucidate native physiological roles of specific heteromeric ion channel isoforms at the cellular, circuit, and systems level.

Author contributions: S.C., R.K.F.-U., B.L.d.G., R.W.T., B.M.O., and H.T. designed research; S.C., R.K.F.-U., D.K., A.M., J.S., W.K., M.J.G., L.S.L., and S.R. performed research; R.J.F. contributed new reagents/analytic tools; S.C., R.K.F.-U., D.K., A.M., J.S., W.K., M.J.G., L.S.L., S.R., R.W.T., B.M.O., and H.T. analyzed data; and S.C., R.K.F.-U., D.K., W.K., B.L.d.G., R.W.T., B.M.O., and H.T. wrote the paper.

Reviewers: R.W.A., The University of Texas at Austin; and M.M.T., Colorado State University.

The authors declare no conflict of interest.

[1]S.C. and R.K.F.-U. contributed equally to this work.

[2]To whom correspondence may be addressed. Email: olivera@biology.utah.edu or h.terlau@physiologie.uni-kiel.de.

This article contains supporting information online at www.pnas.org/lookup/suppl/doi:10.1073/pnas.1813161116/-/DCSupplemental.

Published online December 28, 2018.

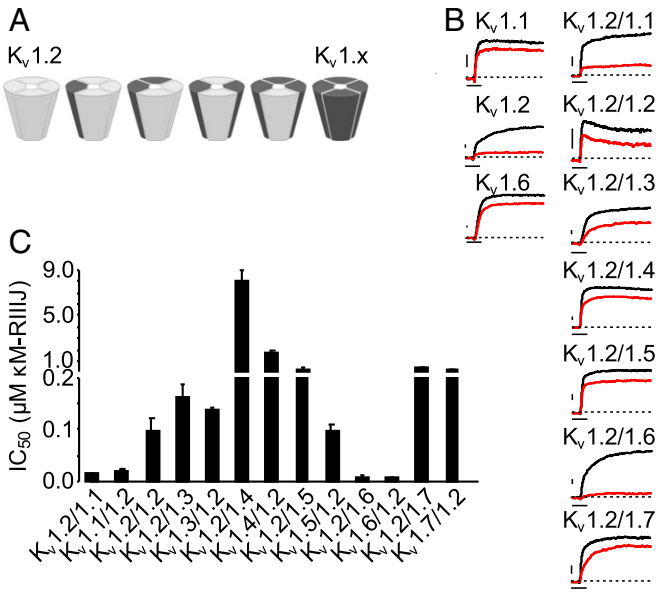

Fig. 1. κM-RIIIJ blocks homomeric and heteromeric Kv1 channels. (*A*) Schematic representation of all possible combinations between two different K_v1 subunits. Homomeric and heteromeric channels containing $K_v1.2$ α-subunits and a second other K_v1 family ($K_v1.x$) subunit are displayed. Similar combinations are possible for all $K_v1.x$ subunits with up to four different subunits forming a functional channel. (*B*) κM-RIIIJ block of homo- and heterodimeric K_v1 channels. Current traces in control (black) and in the presence of κM-RIIIJ (red) are shown. (*Left*) At 1 μM, κM-RIIIJ blocks homomeric $K_v1.1$ and $K_v1.6$ with low apparent affinity (IC_{50} ~ 3–5 μM), whereas it displays ~10× higher potency for $K_v1.2$ homomers (IC_{50} ~ 300 nM). (*Right*) Representative dimeric channel-mediated currents in control and 100 nM κM-RIIIJ evidencing stronger block of $K_v1.2/1.1$ and $K_v1.2/1.6$ channels. Due to extreme differences in apparent affinity, 50 nM κM-RIIIJ is shown for $K_v1.2/1.1$ and 2 μM for $K_v1.2/1.4$. Dashed lines indicate zero current. (Scale bars, 500 pA and 10 ms.) (*C*) κM-RIIIJ affinity toward Kv1.2-containing dimeric K_v1 channels. The bar diagram presented summarizes κM-RIIIJ IC_{50}s for dimeric constructs in forward or reversed order. In comparison with homomeric $K_v1.2$ channels, κM-RIIIJ has a 10- to 20-fold higher affinity for heterodimeric channels composed of $K_v1.2$ and either $K_v1.1$ or $K_v1.6$ subunits. All other dimeric constructs are blocked similarly or less strongly than homomeric $K_v1.2$. The order of the subunits in the concatemers bears no major influence on κM-RIIIJ's activity.

heteromeric K_v channels instead of the symmetric $K_v1.2$ homomer as previously reported.

Thus, this study has important general implications: if natural products like venom-derived peptides evolved to target native voltage-gated K^+ channels, their highest-affinity targets may well be heteromeric combinations. Accordingly, naturally evolved K^+ channel-targeted ligands like κM-RIIIJ may be key to determining the composition and function of heteromeric voltage-gated K^+ channels in biological systems.

Results

κM-RIIIJ Preferentially Targets Heteromeric K_v Channels.

Block of homomeric K_v1 channels. As previously noted, assessing the vast diversity of potential K_v1 channel combinations is a formidable endeavor, as represented by the schematic (Fig. 1*A*) of the combinations possible from only two different subunits. In this work we investigated the effects of κM-RIIIJ on evoked K^+ currents of homotetrameric $hK_v1.1$–7 channels and their heterodimeric combinations by patch clamp on HEK293 cells. Whole-cell current recordings of homomeric channels revealed that κM-RIIIJ affects $K_v1.2$ channels with an IC_{50} of about 300 nM, whereas all other K_v1 channels showed IC_{50}s in the μM range or were not blocked at all ($K_v1.4$ and $K_v1.5$; *SI Appendix*, Table S1). These results are in agreement with those reported previously from two-electrode voltage clamp in *Xenopus* oocytes (1) and demonstrate that κM-RIIIJ displays ~10-fold higher apparent affinity for homomeric $K_v1.2$ channels than for other K_v1 channels including $K_v1.1$ and $K_v1.6$ (IC_{50}s ~ μM).

Block of K_v1 heterodimeric channels. Dimeric concatemers composed of one $K_v1.2$ α-subunit linked to a $K_v1.x$ (x = Kv1.1–7) were constructed. The stoichiometry and arrangement of subunits was controlled by generating two sets of concatemers, in which Kv1.2 provided either the free N-terminal of the dimer ($K_v1.2/K_v1.x$) or the free C-terminal of the dimer ($K_v1.x/K_v1.2$), thus forming heterodimeric channels (A/B-A/B or B/A-B/A). Whole-cell patch-clamp experiments evidenced robust expression of all constructs in HEK293 cells (Fig. 1*B*) after 24–48 h. As readily seen in Fig. 1*B* (*Right*), 100 nM κM-RIIIJ (red traces) blocked the various $K_v1.2/K_v1.x$ heterodimeric constructs with remarkable differences in potency.

From the summary bar graph in Fig. 1*C*, various important points emerge.

i) Steric constraints imposed by the concatemerization, per se, have negligible effects on κM-RIIIJ binding, based on the similar IC_{50}s of homotetramers formed by monomeric $K_v1.2$ α-subunits and those assembled by the linked homodimers (98.3 ± 24.3 nM, n = 7; see *SI Appendix*, Table S2).

ii) For certain heterodimer pairs, reversing monomer order has minimal effect. $K_v1.2/1.3$ and $K_v1.3/1.2$ dimers show comparable IC_{50} values of 165 ± 22 nM (n = 5) and 138 ± 3 nM (n = 2), respectively, as well as $K_v1.2/1.7$ (370 ± 19 nM, n = 4) and $K_v1.7/1.2$ (267 ± 38 nM, n = 3). This suggests that reversing order of monomers within these heterodimers yields similar binding surfaces for the κM-RIIIJ. Similarly, $K_v1.2/1.5$ dimers were blocked slightly less potently than those formed by $K_v1.5/1.2$ (287 ± 163 nM, n = 3, vs. 99 ± 11 nM, n = 4, respectively), suggesting κM-RIIIJ's minimal ability to distinguish between these two different arrangements. Furthermore, κM-RIIIJ displayed modest block of heterodimers of $K_v1.2/1.4$ and $K_v1.4/1.2$ (IC_{50}: 8.1 ± 2 μM, n = 3 and 1.6 ± 2.6 μM, n = 5, respectively), similar to the homomeric channel screen.

iii) In striking contrast, the apparent affinity of κM-RIIIJ for heterodimers $K_v1.2/1.1$ (14.3 ± 2.6 nM, n = 7) and $K_v1.1/1.2$ (18.4 ± 6 nM, n = 10) was significantly increased in comparison with their homotetramers. Similarly, the heterodimeric $K_v1.2/1.6$ and $K_v1.6/1.2$ were strongly blocked by κM-RIIIJ with IC_{50}s of 8.7 ± 2.1 nM (n = 14) and 6.1 ± 1.7 nM (n = 9). Thus, the apparent affinity of κM-RIIIJ toward heterodimers containing $K_v1.2$ is greatly influenced by the subunit composition in the heterodimeric complexes. Furthermore, the observed increase in the apparent affinity of κM-RIIIJ for some of the channels generated as linked concatemers provides a functional readout implying their correct assembly in the plasma membrane.

In summary, heterodimerization of $K_v1.3$–5 and $K_v1.7$ α-subunits with $K_v1.2$ results in ~10-fold increase in κM-RIIIJ's apparent affinity for the complex. Most dramatically, K^+ currents mediated by dimers of $K_v1.2$ with either $K_v1.1$ or $K_v1.6$ are blocked >100-fold more potently than those flowing through their homomeric counterparts.

Block of K_v1 "asymmetric" heterotetramers. The higher affinity of κM-RIIIJ for heterodimeric $K_v1.2/K_v1.1$ and $K_v1.2/K_v1.6$ channels, relative to their homomeric counterparts, demonstrates that relatively small differences in the binding surface of the target channel are critical to κM-RIIIJ's activity. Functional K_v channels are formed by four independent α-subunits; therefore, a binomial arrangement of two α-subunits will have any of those subunits occupying any position of the tetramer. Thus, "symmetric" (2:2 = AABB or ABAB) or "asymmetric" channels composed of 3xA and 1xB (and vice versa) are possible. This flexibility would result in significantly different molecular recognition surfaces exposed to peptide toxins like κM-RIIIJ, which we set out to explore by generating binomial concatemers of $K_v1.2$ and either $K_v1.1$ or $K_v1.6$, in 2:2 and 3:1 stoichiometry, and linked in different orders.

The correct and complete synthesis of the constructs used throughout this work was verified by immunodetection by an anti-$K_v1.2$ antibody in Western blot experiments. Fig. 2*A* shows an experiment, in which the protein products of representative constructs expressed in HEK293 cells were electrophoresed and immunoblotted. In this figure, clear bands at 75, 150, and 300 kDa report on monomeric, dimeric, and tetrameric channels, respectively, of expected molecular weight, as each homomer is ∼75 kDa.

Fig. 2*B* exhibits representative currents of binomial constructs composed of $K_v1.2$ and $K_v1.6$ channels of different stoichiometry and arrangement. The colored traces were recorded in the presence of 0.5 nM (red) and 5 nM (blue) κM-RIIIJ, showing that those currents mediated by the asymmetric (3:1) channel (*Right*) were preferentially blocked in comparison with the symmetric dimer of dimers (2:2; *Left*).

The bar graph in Fig. 2*C* condenses our analysis of symmetric and asymmetric channels exposed to conotoxin κM-RIIIJ. The equal inhibition of symmetric $K_v1.6/1.2/1.6/1.2$ and $K_v1.6/1.2/1.2/1.6$ channels (IC_{50}: 13.6 ± 3.6 nM, $n = 4$ and 15.9 ± 4.2 nM, $n = 3$, respectively) shows that the "order" of the two subunits does not alter κM-RIIIJ binding. In contrast, analysis of the tetrameric concatemers that presented an asymmetric surface (3:1 stoichiometry) revealed that such configuration was determinant to high-affinity κM-RIIIJ binding. Hence, the apparent affinity of κM-RIIIJ for $K_v1.1/1.2/1.2/1.2$ channels was 1.2 ± 0.3 nM ($n = 8$), while only 0.5 ± 0.1 nM ($n = 14$) κM-RIIIJ was sufficient to block 50% of the $K_v1.6/1.2/1.2/1.2$ mediated currents (Fig. 2 *B* and *C*). These results demonstrate that the apparent affinity of κM-RIIIJ for heteromeric Kv1 channels consisting of $K_v1.2$ and either $K_v1.1$ or $K_v1.6$ is higher when the tetrameric channel contains only one subunit of either $K_v1.1$ or $K_v1.6$ as opposed to two. This shows that although the apparent affinity to homomers of $K_v1.1$ or $K_v1.6$ is lower by one order of magnitude compared with those of $K_v1.2$, the sole presence of one such subunit, either $K_v1.1$ or $K_v1.6$, is sufficient to cause a >100-fold enhancement in the affinity of κM-RIIIJ for the K_v1 complex. The observed increased sensitivity of the linked concatemeric proteins to κM-RIIIJ provides a functional readout of their correct assembly in the plasma membrane.

Furthermore, these findings show that the asymmetric surface of K_vs composed of three $K_v1.2$ and one $K_v1.1/K_v1.6$ is highly favorable to κM-RIIIJ binding. Thus, the graded effects of κM-RIIIJ are an accurate correlate to the channel composition and stoichiometry, representing a valuable tool in the study of neuronal voltage-gated K_v channels.

Molecular Insights into κM-RIIIJ Binding to Asymmetric Kv1 Heteromers. Functionally, inclusion of one subunit of either $K_v1.1$ or $K_v1.6$ leads to a profound increase in κM-RIIIJ's affinity for $K_v1.2$-containing channels. Sequence alignment of the Shaker and Kv1 pore regions is shown in Fig. 3*A*. Visual inspection reveals that $K_v1.1$ and $K_v1.6$ distinguish themselves from the other K_v1s in that a tyrosine (Y379 and Y429, respectively) resides in the homologous position of Shaker T449, known to be critical for extracellular binding of several substances including tetraethylammonium (2). Previous studies on κM-RIIIK (a close relative of κM-RIIIJ) described it as a pore-blocking peptide (3–5), and therefore we surmised κM-RIIIJ would exert its inhibitory actions by interacting with the same channel region. Hence, a tyrosine residue was introduced in the homologous position of $K_v1.4$ (K531Y) within the heterodimer $K_v1.2/K_v1.4$, and the reciprocal mutation was made in $K_v1.6$ in $K_v1.2/K_v1.6$. Fig. 3*B* provides examples of current traces of the wild-type and pore mutant dimers $K_v1.2/K_v1.4$-K531Y and $K_v1.2/K_v1.6$-Y429K. Exposure to 10 nM κM-RIIIJ (red) clearly highlights the importance of such tyrosine within the heteromeric pores. Thus, $K_v1.2/K_v1.4$-K531Y is blocked with an IC_{50} of 9 ± 0.7 nM ($n = 5$), in stark contrast with its wild-type counterpart (8.1 ± 2 μM, $n = 5$). Accordingly, the mutant heterodimer $K_v1.2/K_v1.6$-Y429K significantly lost sensitivity to κM-RIIIJ (IC_{50} 2.0 ± 0.2 μM, $n = 4$). Thus, an apparent affinity increase of ∼1,000-fold for $K_v1.2/K_v1.4$-K531Y and the ∼250-fold decrease in binding affinity for $K_v1.2/K_v1.6$-Y429K demonstrate that (*i*) a tyrosine residue within the heteromeric pore is a major determinant of κM-RIIIJ's potency; and (*ii*) κM-RIIIJ intimately interacts with the K_v channel pore.

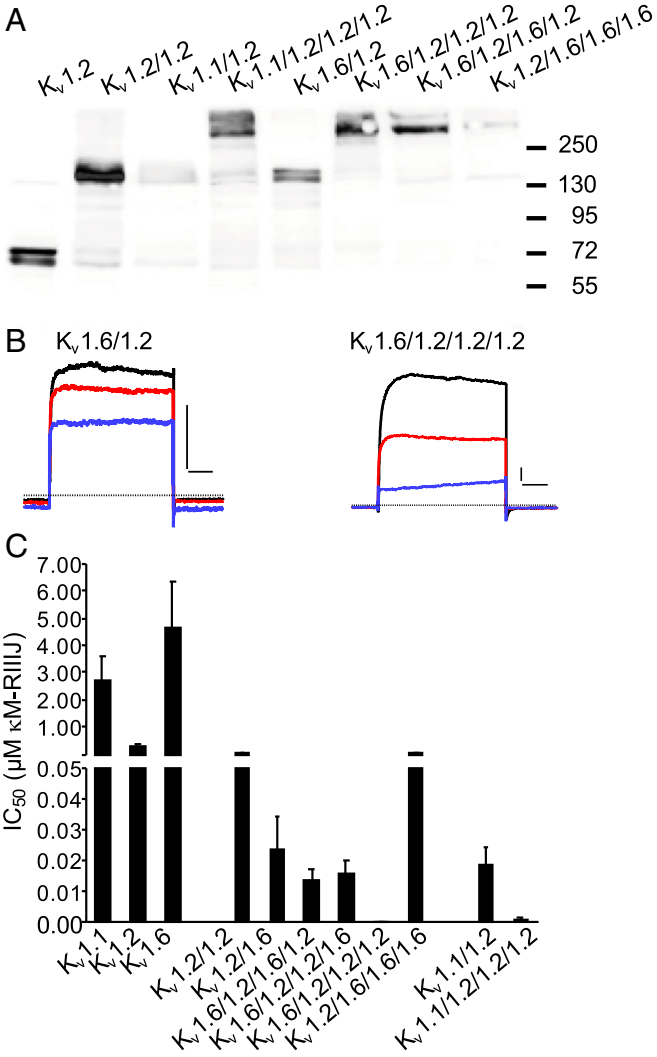

Fig. 2. κM-RIIIJ displays enhanced apparent affinity toward asymmetric K_v1 channels. (*A*) Western blot analysis of selected concatemeric constructs expressed in HEK293. Bands corresponding to 75-, 150-, and 300-kDa protein products were recognized by an anti-Kv1.2 antibody evidencing expression of monomeric, dimeric, and tetrameric channels, respectively. (*B*) Representative current traces of symmetric heterodimeric and asymmetric heterotetrameric channels composed of $K_v1.2$ and $K_v1.6$. The effect of 0.5 nM (red) and 5 nM (blue) κM-RIIIJ on evoked K^+ currents from $K_v1.6/1.2$ dimer and tetrameric concatemers composed of three $K_v1.2$ subunits and one $K_v1.6$ subunit are shown (black: control). The zero current level is marked by the dashed line. (Scale bars, 1 nA and 50 ms.) (*C*) IC_{50}s of κM-RIIIJ block of homomeric and heteroconcatemeric K_v1 channels formed by $K_v1.1$, $K_v1.2$, and $K_v1.6$ subunits in different combinations. κM-RIIIJ displayed extremely high apparent affinity (sub-nM) for asymmetric concatemers composed of one $K_v1.1$ or $K_v1.6$ subunit together with three $K_v1.2$ subunits (*SI Appendix*, Table S2).

Introducing the equivalent K/Y mutation in the asymmetric $K_v1.2/1.2/1.2/1.4$ concatemer results in 200-fold higher affinity of κM-RIIIJ for $K_v1.2/1.2/1.2/1.4$-K531Y channels, corroborating the crucial role of this amino acid for peptide-binding strength to asymmetric channel complexes (*SI Appendix*, Fig. S1).

A global perspective of κM-RIIIJ association with asymmetric heterotetramers was obtained by molecular dynamics simulations. For this, the biological assembly of $K_v1.2$'s crystal structure (3LUT, pore residues 311–421) served as a template where the asymmetry-imposing subunits ($K_v1.6$ and $K_v1.1$) were

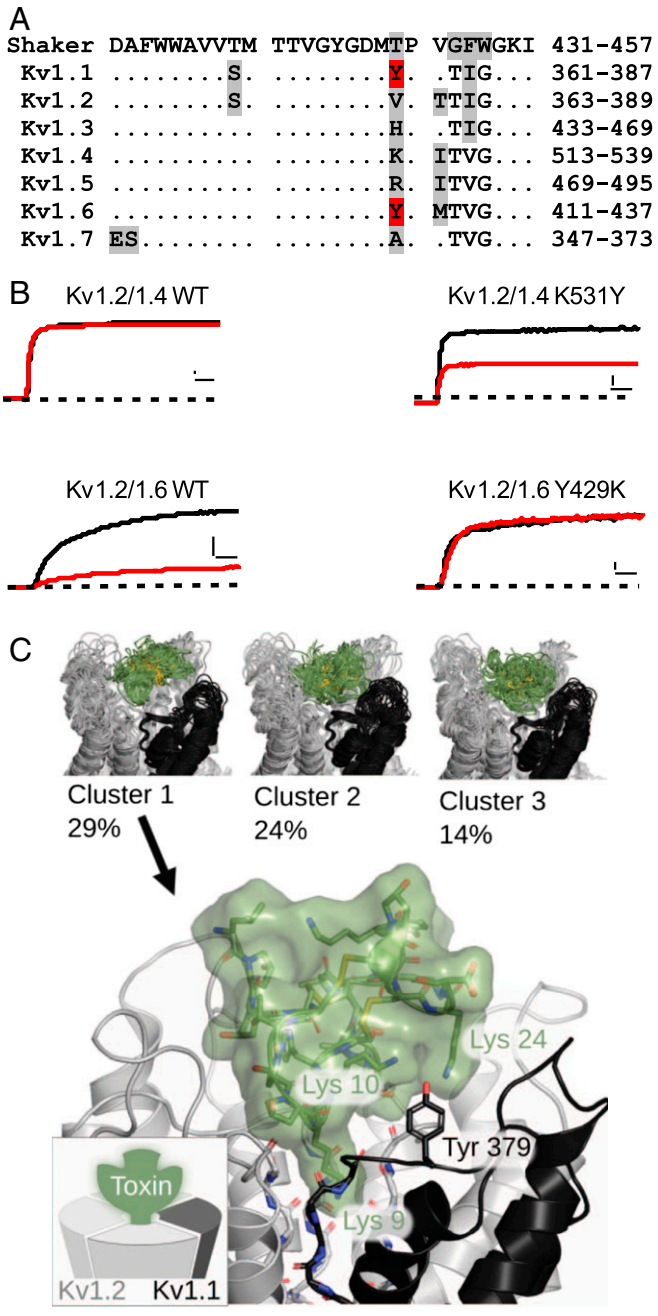

Fig. 3. Binding of κM-RIIIJ to the K_v1 channel pore. (*A*) Pore region sequence alignment of Shaker and K_v1 channel subunits. Observe that in $K_v1.1$ and $K_v1.6$ there is a tyrosine (Y379 and Y429, respectively, in red) homologous to Shaker T449. Identical amino acids to Shaker are shown as dots. Amino acids that differ from the majority are shaded in gray. (*B*) Tyrosine incorporation into a κM-RIIIJ–resistant dimer $K_v1.2/1.4$ renders it highly sensitive. The 10 nM κM-RIIIJ hardly affects $K_v1.2/1.4$ mediated currents (*Top Left*), whereas the same [κM-RIIIJ] leads to a profound block of $K_v1.2/1.4$-K531Y mediated currents (*Top Right*). Accordingly, $K_v1.2/1.6$ mediated currents are potently blocked by 10 nM of κM-RIIIJ, whereas sensitivity to the same [κM-RIIIJ] was abolished in the reciprocal mutant $K_v1.2/1.6$-Y429K. These results underscore the importance of the bulkier aromatic residue (tyrosine) at this position for κM-RIIIJ's high-affinity binding. Zero current is indicated by the dashed line. [Scale bars, 2 nA (dimeric-WT), 200 pA (dimeric mutants), and 10 ms.] (*C*) Molecular dynamics simulation for κM-RIIIJ binding to $K_v1.2/1.2/1.2/1.1$ heterotetramer. Trajectories have been clustered to reveal different κM-RIIIJ docking positions. Visualization of the largest cluster (constituting 29% of the observed poses) is shown in more detail. $K_v1.2$ subunits are colored gray in cartoon representation, while the $K_v1.1$ subunit is black. κM-RIIIJ is represented by the green licorice and surface. κM-RIIIJ-Lys9 interacts with the channel selectivity filter (blue) occluding the permeation pathway, while Lys10 and Lys24 interact with Kv1.1-Tyr379 (homologous to Kv1.6-Tyr429).

homology-modeled and incorporated. The structure of κM-RIIIJ was based on similarity to κM-RIIIK (*Methods*), and interaction to $K_v1.6/1.2/1.2/1.2$ and $K_v1.1/1.2/1.2/1.2$ was assessed in silico. As depicted in Fig. 3*C*, molecular dynamic simulation returned three major clusters (29–14% likelihood, *Top*) where the likely orientation of κM-RIIIJ within the asymmetric pore indicates that lysine 9 (from κM-RIIIJ) orients itself into the channel's permeation pathway. Fig. 3*C*, *Bottom*, provides an expanded view of Cluster 1 where K24 and K10 (κM-RIIIJ) are in close vicinity of the critical pore tyrosine from $K_v1.1$ (Y379) and $K_v1.6$ (Y429) in agreement with the functional data compiled here.

In addition, the observed role of positively charged Lys residues in κM-RIIIJ affords a mechanistic explanation toward weak binding to most of the channels containing $K_v1.4$ or $K_v1.5$ subunits. Homomeric $K_v1.4$ and $K_v1.5$, as well as heterodimers of $K_v1.2$ and $K_v1.4$, are modestly blocked by κM-RIIIJ, with the exception of heterodimers including $K_v1.5$, toward which κM-RIIIJ displayed higher affinity. These subunits have basic amino acids at the homologous position of Tyr in $K_v1.1$ and $K_v1.6$ ($K_v1.4$ K531 and $K_v1.5$ R487; Fig. 3*A*), which may exert repulsive forces over the toxin's positively charged moieties. As shown by the electrophysiological experiments, eliminating the charge of this position in heterodimeric and tetrameric constructs restores the toxin affinity for the heteromeric constructs, further underpinning the significance of electrostatic interactions in κM-RIIIJ binding.

κM-RIIIJ Distinguishes Between DRG Neuron Subtypes. Sensory neurons in the dorsal root ganglia (DRG) express various members of the K_v1 family of K^+ channels. However, the functional and pharmacological similarities between homomeric K^+ channels mediated by close family relatives like $K_v1.1$, $K_v1.2$, and $K_v1.6$ has hindered the assignment of precise molecular correlates to the native currents observed in DRGs. An exquisitely tuned peptide like κM-RIIIJ provides the opportunity to distinguish neurons in which homo- or heteromeric K_v1 channel populations are expressed, based on their sensitivity to this conotoxin. We took advantage of the high-content Ca^{2+}-imaging approach known as constellation pharmacology (6, 7) to explore the question posed. Fig. 4 provides a snapshot of one such experiment, in which dissociated mouse DRG neurons were loaded with Fura-2-AM and subjected to various concentrations of κM-RIIIJ and the $K_v1.1$-selective blocker, Dtx-K, before depolarizing stimuli. Fig. 4*A* displays stereotyped Ca^{2+} responses to depolarization with high $[K^+]_0$ that return to baseline on K^+ removal, from four different neurons where neither of the toxins caused apparent changes in the Ca^{2+} signal. The four neurons from Fig. 4*B* (each had a cross-sectional cell area ~450 μm^2), however, robustly responded to the presence of three different concentrations of κM-RIIIJ (low: 25 nM and 75 nM; high: 1 μM), as well as to 100 nM Dtx-K by displaying enhanced Ca^{2+} peaks. The reaction of these neurons to low [κM-RIIIJ] indicates that in these cells, K_v currents are likely mediated by heteromeric channels composed of $K_v1.2$ subunits and those with Dtx-K sensitive $K_v1.1$ subunits, as a plausible partner. Therefore, we can postulate that this medium-diameter DRG neuronal cell population expresses $K_v1.1/1.2$ heteromeric channels. Furthermore, the Ca^{2+} responses shown in Fig. 4*C* were obtained from small (each had a cross-sectional cell area ~250 μm^2) DRG cells that only responded to the high dose of κM-RIIIJ suggesting a population where Kv1.2 homotetramers or low-affinity heterotetramers are the dominant channels expressed.

Discussion

The physiological role of heteromeric K_v channels has rarely been explored due to the lack of reliable pharmacological tools. From

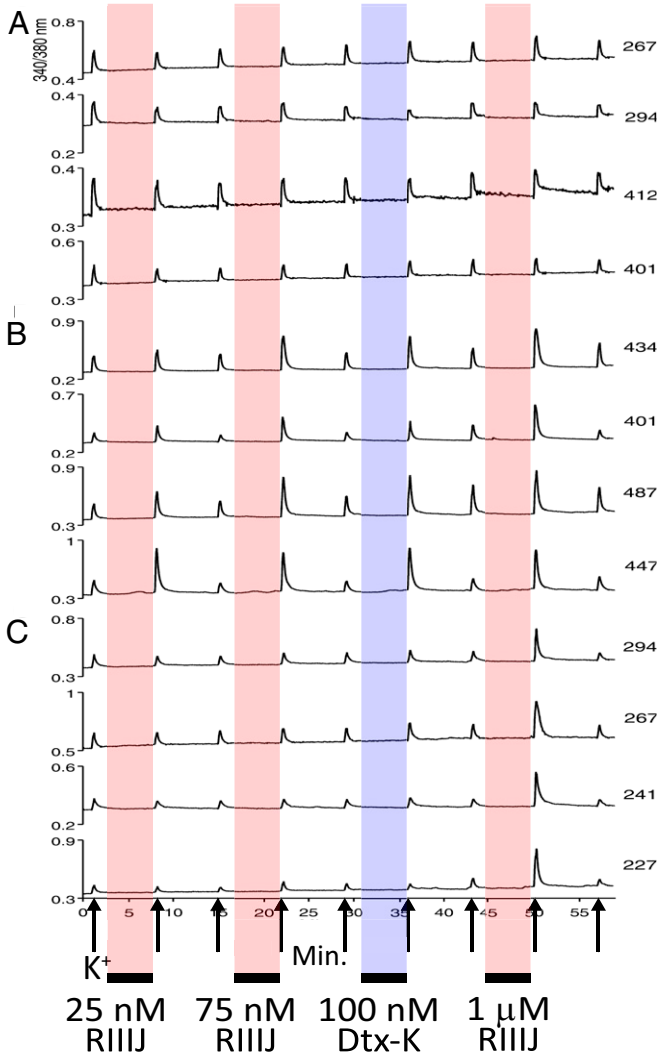

Fig. 4. κM-RIIIJ can distinguish between different sensory neuron subtypes. Representative calcium-imaging traces from three DRG neuronal subclasses displaying distinct responses to κM-RIIIJ and Dtx-K. (*A*) Neurons unaffected by κM-RIIIJ or Dtx-K: Four representative neurons unaltered by the application of κM-RIIIJ (25 nM, 75 nM, and 1 μM) and Dtx-K (100 nM), suggesting the lack of functional expression of $K_v1.1$ and $K_v1.2$ channels in these neurons. (*B*) Neurons responsive to the application of low [κM-RIIIJ]. The examples shown correspond to neurons that displayed an increase in peak height following a depolarizing stimulus in the presence of 25 nM, 75 nM, and 1 μM κM-RIIIJ and 100 nM Dtx-K, indicating the presence of both $K_v1.1$ and $K_v1.2$ channels in these neurons. (*C*) Neurons exclusively responsive to high [κM-RIIIJ]. These neurons were not affected by the application of low doses (25 and 75 nM) of κM-RIIIJ nor 100 nM Dtx-K but displayed increases in peak height after exposure to 1 μM κM-RIIIJ. The low sensitivity to κM-RIIIJ and insensitivity to Dtx-K suggest the presence of homotetrameric $K_v1.2$ channels and the absence of homomeric $K_v1.1$ or heteromeric $K_v1.1/1.2$ complexes in this cell population. Each trace corresponds to individual cells. The *x* axis is time (in minutes), and the *y* axis tracks the ratio of relative fluorescence change (ΔF/F) excited at 340 and 380 nM. Upward arrows mark the application of the depolarizing stimulus (20 mM $[K^+]_o$, ∼15 s). Colored boxes (red: κM-RIIIJ; blue: dendrotoxin-K) indicate the time of peptide exposure (∼6 min) in between the applications of depolarizing stimulus. Numbers to the right indicate cell area in μm^2.

the multiple cone snail toxins that interact with K_v channels, κM-RIIIJ was shown to interact with homomeric $K_v1.2$ channels in *Xenopus* oocytes. Here, we offer evidence of κM-RIIIJ's preferential (>100-fold) inhibition of heteromeric channels composed of three $K_v1.2$ and one $K_v1.1$ or $K_v1.6$ α-subunits. We have identified crucial molecular interactions between κM-RIIIJ and the K_v1 channel pore that provide a rationale for the exquisite selectivity and potency of κM-RIIIJ for asymmetric K_v1 heteromers. Finally, use of κM-RIIIJ in constellation pharmacology (6, 7) experiments pinpointed identifiable subpopulations of mouse DRG neurons with distinct functional $K_v1.2$-containing channel subsets.

Heteromeric K_v Channels. Although different K_v1 subunits have been identified in various cell types, most studies rely on immunodetection of channel proteins or mRNA (qPCR, hybridization probes), which do not provide accurate information about the actual composition of multisubunit complexes like heteromeric K_v1 channels at the single-cell level. In the CNS, several heteromeric combinations of $K_v1.2$ with either $K_v1.1$ or $K_v1.6$ have been proposed. An elegant but laborious immunoprecipitation study used antibodies to systematically deplete individual K_v subunits from tissue homogenates, revealing the presence of multiple heteromeric K_v channels in the human CNS (8). In this study, the existence of $K_v1.1/K_v1.2$ heteromeric channels in cortical gray matter, white matter, and spinal cord (8) was inferred in good agreement with our Ca^{2+}-imaging results.

Additional studies using specific antibodies against various K_v1s demonstrated that K_v1 channels are predominantly found in neuronal cells within the mammalian brain. The K_v1 subunits most abundantly detected in human brain are $K_v1.1$, $K_v1.2$, and $K_v1.4$ [for review, see Trimmer and Rhodes (9) and Vacher et al. (10)], and often $K_v1.1$ colocalizes with either $K_v1.2$ or $K_v1.4$ in support of the existence of heteromeric K_v1 channels in the brain. Examples of colocalization of $K_v1.1$ and $K_v1.2$ in the absence of $K_v1.4$ occur in cerebellar basket cell terminals, the juxtaparanodal membrane (node of Ranvier), and in axon terminal segments. $K_v1.6$ seems to be found less abundantly and predominantly in interneurons. However, throughout the whole brain, some $K_v1.6$ staining appears on principal cell dendrites where $K_v1.2$ and $K_v1.1$ are also present (11).

Little is known about heteromeric K_v1 complexes in nonneuronal tissue and, particularly, in the heart the functional importance of heteromeric K_v1s has received little attention. A previous report from our laboratory showed that, unlike κM-RIIIJ, κM-RIIIK is cardioprotective in a rodent model of ischemia/reperfusion, despite its comparatively weaker block of homomeric $K_v1.2$ (1). Differential activity of these peptides on $K_v1.2$ heterodimeric channels provided a plausible explanation for disparate effects in such closely related peptides. The results presented in this study corroborate our previous findings in that the higher-affinity targets of κM-RIIIJ are composed of subunits not abundantly found in cardiomyocytes [for overview, see Nerbonne and Kass (12)]. Curiously, $K_v1.1$, $K_v1.2$, and $K_v1.6$ have been immunodetected in sinoatrial node cells in ferret hearts (13).

Our data suggest that the likely "natural" targets of κM-RIIIJ actions are neurons containing $K_v1.2/K_v1.1$ or $K_v1.2/K_v1.6$ heteromers, which would be congruent with the potential role of κM-RIIIJ in prey capture as a part of the "lightning strike cabal" (14). Our experiments identifying different subpopulations of DRG neurons by their responses to either low or high [κM-RIIIJ] strongly support the notion of $K_v1.2$ subunits as part of hetero- and homomeric K^+ channels in the peripheral nervous system.

Asymmetric K_v1 Channel. It is remarkable that κM-RIIIJ preferentially inhibits asymmetric K_v channels with 1:3 stoichiometry. Other channel families that assemble in tetramers composed of two related subunits in 3:1 stoichiometry may be of physiological importance. Such is the case of the modulatory K_v α-subunit $K_v9.3$, which does not form functional homotetramers, but participates in heteromeric arrangements of $3xK_v2.1$ and $1xK_v9.3$ subunits (15). The molecular determinants of heteromeric cyclic nucleotide-gated (CNG) channels of 3xCNGA1 and 1xCNGB1 have been described elsewhere (16, 17). Thus, it is plausible to anticipate that many other heteromeric K^+ channels of asymmetric composition exist in nature. This would imply that such nonsymmetric arrangement of functional channels delineates a

correspondingly asymmetric permeation pathway of significant pharmacological standing. In line with our findings, previous work showed that the affinity of TEA to Kv1.1/Kv1.2 concatemers is affected by the subunit ratio (18). Therefore, asymmetric ion channel compositions should be taken into account in the development of K_v channel-targeted substances of therapeutic potential.

κM-RIIIJ: A Tool for the Study of Heteromeric Kv1 Channels. Our work in heterologous systems underpins the potential of κM-conotoxin RIIIJ as a valuable diagnostic tool for the identification of functional K_v1 channel complexes according to their sensitivity to this conotoxin. We verified κM-RIIIJ's ability to distinguish among peripheral neuron subclasses expressing distinct heteromeric K_v channels by constellation pharmacology. We used the K_v1.1-selective blocker Dendrotoxin-K to identify DRG neuronal cells in which heteromeric channels formed by K_v1.1 and K_v1.2 constitute a major component of the I_{KDR} in these cells. Results presented throughout this paper highlight the advantages of using conotoxins and, particularly, κM-RIIIJ, as pharmacological tools to enable the study of functioning heteromeric K_v channels in living cells.

Materials and Methods

Conotoxin κM-RIIIJ was synthesized as described by Chen et al. (1). The K_v1 channels used here correspond to the human isoforms: K_v1.1 (hKCNA1; NM_000217), K_v1.2 (hKCNA2; NM_004974), K_v1.3 (hKCNA3; NM_002232), K_v1.4 (hKCNA4; NM_002233), K_v1.5 (hKCNA5; NM_002234), K_v1.6 (hKCNA6; NM_002235), and K_v1.7 (hKCNA7; NM_031886).

Molecular Biology. cDNAs coding hK_v1.1–7 α-subunits were subcloned into pcDNA3.1 for expression in HEK293 cells. Dimeric concatenated K_v1 subunits were generated by replacement of the stop (anterior subunit) and start codons (posterior subunit) by AatII restriction sites according to the QuikChange Site directed Mutagenesis method (Stratagene). Tetrameric concatemers were built by fusion of dimeric constructs, in which the stop (anterior dimer) and start codons (posterior dimer) were replaced by an XhoI restriction site. All constructs were verified by sequencing.

Cell Culture and Electrophysiological Recordings. All electrophysiological measurements were done with transiently transfected HEK293 cells in the whole-cell configuration of the patch-clamp technique at room temperature. For more detail, see *SI Appendix, Supplementary Methods*.

Western Blot. Western blotting was performed by using monoclonal antibodies to K_v1.2 (NeuroMab monoclonal mouse K14/16; #75–008; 1:20,000). For more detail, see *SI Appendix, Supplementary Methods*.

Molecular Dynamics Simulations. All simulations were done with GROMACS 4.6 (19–22), the amber99sb force field (23), and the SPC/E water model (24), at constant 320 K [v-rescale thermostat (25)] and pressure of 1 bar [Berendsen Barostat (26)]. Parameters used for lipids were from Berger et al. (27), and the appropriate ions were from Joung and Cheatham (28).

K_v channel models were based on the full-length K_v1.2 crystal structure [PDB ID: 3LUT (29)]; the pore region (aa 311–421) of chimeric channels was modeled with Modeler9.8 (30, 31) by exchanging one K_v1.2 monomer with the aligned sequence of K_v1.1 and K_v1.6, respectively. The model of κM-conotoxin RIIIJ was generated by Modeler9.8 from the solution NMR structure of κM-RIIIK (4). For more detail, see *SI Appendix, Supplementary Methods*.

Constellation Pharmacology: Calcium Imaging. The experimental methods of constellation pharmacology have been described in detail previously (6, 7, 32, 33). For more detail, see *SI Appendix, Supplementary Methods*.

Data Analysis. IC_{50} values were calculated according to $IC_{50} = [\text{toxin}]/(I_{ctrl}/I_{toxin} - 1)$ where [toxin] is the applied concentration of toxin; I_{ctrl} is the current amplitude before toxin; and I_{toxin} is the current after toxin application. All data are presented as mean ± SEM (*n*), where *n* is the number of biological replicates.

ACKNOWLEDGMENTS. This work was supported by the University of Kiel and by Grant GM 48677 (to B.M.O.) from the National Institute of General Medical Sciences. This work was also supported by Canadian Institutes of Health Research, CIHR MOP-10053, and National Science and Engineering Research Council (Canada) NSERC RGPIN-2012-418658-2012 (to R.J.F.).

1. Chen P, Dendorfer A, Finol-Urdaneta RK, Terlau H, Olivera BM (2010) Biochemical characterization of kappaM-RIIIJ, a Kv1.2 channel blocker: Evaluation of cardioprotective effects of kappaM-conotoxins. *J Biol Chem* 285:14882–14889.
2. MacKinnon R, Yellen G (1990) Mutations affecting TEA blockade and ion permeation in voltage-activated K+ channels. *Science* 250:276–279.
3. Ferber M, Al-Sabi A, Stocker M, Olivera BM, Terlau H (2004) Identification of a mammalian target of kappaM-conotoxin RIIIK. *Toxicon* 43:915–921.
4. Al-Sabi A, et al. (2004) KappaM-conotoxin RIIIK, structural and functional novelty in a K+ channel antagonist. *Biochemistry* 43:8625–8635.
5. Verdier L, et al. (2005) Identification of a novel pharmacophore for peptide toxins interacting with K+ channels. *J Biol Chem* 280:21246–21255.
6. Teichert RW, et al. (2012) Functional profiling of neurons through cellular neuropharmacology. *Proc Natl Acad Sci USA* 109:1388–1395.
7. Teichert RW, et al. (2012) Characterization of two neuronal subclasses through constellation pharmacology. *Proc Natl Acad Sci USA* 109:12758–12763.
8. Coleman SK, Newcombe J, Pryke J, Dolly JO (1999) Subunit composition of Kv1 channels in human CNS. *J Neurochem* 73:849–858.
9. Trimmer JS, Rhodes KJ (2004) Localization of voltage-gated ion channels in mammalian brain. *Annu Rev Physiol* 66:477–519.
10. Vacher H, Mohapatra DP, Trimmer JS (2008) Localization and targeting of voltage-dependent ion channels in mammalian central neurons. *Physiol Rev* 88:1407–1447.
11. Rhodes KJ, et al. (1997) Association and colocalization of the Kvbeta1 and Kvbeta2 beta-subunits with Kv1 alpha-subunits in mammalian brain K+ channel complexes. *J Neurosci* 17:8246–8258.
12. Nerbonne JM, Kass RS (2005) Molecular physiology of cardiac repolarization. *Physiol Rev* 85:1205–1253.
13. Brahmajothi MV, Morales MJ, Campbell DL, Steenbergen C, Strauss HC (2010) Expression and distribution of voltage-gated ion channels in ferret sinoatrial node. *Physiol Genomics* 42A:131–140.
14. Olivera BM (1997) E.E. Just Lecture, 1996. Conus venom peptides, receptor and ion channel targets, and drug design: 50 million years of neuropharmacology. *Mol Biol Cell* 8:2101–2109.
15. Kerschensteiner D, Soto F, Stocker M (2005) Fluorescence measurements reveal stoichiometry of K+ channels formed by modulatory and delayed rectifier alpha-subunits. *Proc Natl Acad Sci USA* 102:6160–6165.
16. Shuart NG, Haitin Y, Camp SS, Black KD, Zagotta WN (2011) Molecular mechanism for 3:1 subunit stoichiometry of rod cyclic nucleotide-gated ion channels. *Nat Commun* 2:457.
17. Weitz D, Ficek N, Kremmer E, Bauer PJ, Kaupp UB (2002) Subunit stoichiometry of the CNG channel of rod photoreceptors. *Neuron* 36:881–889.
18. Al-Sabi A, Kaza SK, Dolly JO, Wang J (2013) Pharmacological characteristics of Kv1.1- and Kv1.2-containing channels are influenced by the stoichiometry and positioning of their α subunits. *Biochem J* 454:101–108.
19. Hess B, Kutzner C, van der Spoel D, Lindahl E (2008) GROMACS 4: Algorithms for highly efficient, load-balanced, and scalable molecular simulation. *J Chem Theory Comput* 4:435–447.
20. Pronk S, et al. (2013) GROMACS 4.5: A high-throughput and highly parallel open source molecular simulation toolkit. *Bioinformatics* 29:845–854.
21. Van Der Spoel D, et al. (2005) GROMACS: Fast, flexible, and free. *J Comput Chem* 26:1701–1718.
22. Abraham MJ, et al. (2015) GROMACS: High performance molecular simulations through multi-level parallelism from laptops to supercomputers. *SoftwareX* 1–2:19–25.
23. Hornak V, et al. (2006) Comparison of multiple Amber force fields and development of improved protein backbone parameters. *Proteins* 65:712–725.
24. Berendsen HJC, Grigera JR, Straatsma TP (1987) The missing term in effective pair potentials. *J Phys Chem* 91:6269–6271.
25. Bussi G, Donadio D, Parrinello M (2007) Canonical sampling through velocity rescaling. *J Chem Phys* 126:014101.
26. Berendsen HJC, Postma JPM, van Gunsteren WF, DiNola A, Haak JR (1984) Molecular dynamics with coupling to an external bath. *J Chem Phys* 81:3684–3690.
27. Berger O, Edholm O, Jähnig F (1997) Molecular dynamics simulations of a fluid bilayer of dipalmitoylphosphatidylcholine at full hydration, constant pressure, and constant temperature. *Biophys J* 72:2002–2013.
28. Joung IS, Cheatham TE, 3rd (2008) Determination of alkali and halide monovalent ion parameters for use in explicitly solvated biomolecular simulations. *J Phys Chem B* 112:9020–9041.
29. Chen X, Wang Q, Ni F, Ma J (2010) Structure of the full-length Shaker potassium channel Kv1.2 by normal-mode-based X-ray crystallographic refinement. *Proc Natl Acad Sci USA* 107:11352–11357.
30. Fiser A, Do RK, Sali A (2000) Modeling of loops in protein structures. *Protein Sci* 9:1753–1773.
31. Sali A, Blundell TL (1993) Comparative protein modelling by satisfaction of spatial restraints. *J Mol Biol* 234:779–815.
32. Smith NJ, et al. (2013) Comparative functional expression of nAChR subtypes in rodent DRG neurons. *Front Cell Neurosci* 7:225.
33. Teichert RW, Memon T, Aman JW, Olivera BM (2014) Using constellation pharmacology to define comprehensively a somatosensory neuronal subclass. *Proc Natl Acad Sci USA* 111:2319–2324.